Journal of Chromatography
Separation Techniques

Akl et al., J Chromat Separation Techniq 2013, 4:5
DOI: 10.4172/2157-7064.1000185

Research Article Open Access

The Utility of Novel Superabsorbent Core Shell Magnetic Nanocomposites for Efficient Removal of Basic Dyes from Aqueous Solutions

Magda A Akl[1]*, Ayman Atta[2], Abd ElFattah M Youssef[1] and Mohammed A Ibraheim[1]

[1]*Chemistry Department, Faculty of Science, Mansoura University, Mansoura, Egypt*
[2]*Egyptian Petroleum Research Institute, Petroleum Application Department, Nasr City 11727, Cairo, Egypt*

Abstract

A series of novel superabsorbents Fe_3O_4/poly(Acrylamide-co-sodium acrylate) core shell magnetic nanogel based on crosslinked poly (sodium acrylate-co-acrylamide) are investigated for the removal of methylene blue from aqueous solutions. The superabsorbents are characterized by FTIR, HR-TEM and SEM. The adsorbents exhibited high sorption capacities toward basic dyes, *viz*.: 2167.802-2765.893 mg g^{-1}. The adsorption kinetics followed a pseudo-second order equation. Equilibrium isotherm data are analyzed according to Langmuir and Freundlich equations. The thermodynamic parameters including ΔG°, ΔH° and ΔS° for the adsorption processes of MB on the nanocomposite hydrogel were also calculated, and the negative value of ΔG° indicated the spontaneous nature of adsorption.

Keywords: Methylene blue; Nanocomposite Hydrogel; Magnetic nanogel; Temperature

Introduction

AIn recent years, pollution from dye wastewater has become a serious environmental problem due to the vast and increasing uses of a variety of dyes. [1] Methylene blue (MB) is the most commonly used substance for dying cotton, wood and silk. It may cause some hazardous problems to human and animal health [2]. Amongst the numerous techniques of dye removal [3-10], adsorption is a well-known equilibrium separation process and is an effective method for water decontamination applications [11,12].

Recently, there has been an increasing interest in the design and fabrication of magnetic polymeric particles consisting of one or more magnetic nanoparticles as a core with a coating matrix of polymer as a shell. The main advantage of magnetic nanocomposite particles (MCPs) over conventional polymer nanocomposite particles is that, because of their magnetic properties, they can be rapidly separated from the mixtures by magnetic extraction [13]. They have been tried extensively in various fields including industrial water treatment [14,15].

To our best knowledge, there is no literature focusing on the use of Fe3O4/ poly(sodium acrylate co acrylamide) core-shell magnetic nanogel for the removal of MB from aqueous solutions. The objective of this work is to develop crosslinked p(Am-co-Na Ac) nanocomposite hydrogel that contain different amounts of Fe_3O_4/p(Am-co-Na Ac) core–shell magnetic nanogels as potential effective adsorbents to remove MB from aqueous solution attributing to their following unique properties: (i) Fe_3O_4 increase mechanic strength to enhance the usable life. (ii) The p(Am-co-Na Ac) shells with nano-scaled size provide much larger specific surface area. (iii) The raw materials are low-cost and the synthetic approach is simple, which make these nanoparticles potentially commercializable. (iv) These nanoparticles do not cause environmental pollution during the course of treatment.

Experimental

Materials

All chemicals were of analytical grade and used as received, Iron (III) chloride hexahydrate ($FeCl_3.6H_2O$>99%), Iron (II) chloride tetrahydrate ($FeCl_2.4H_2O$>99%) were purchased from Merck. Acrylic acid (AA), acrylamide (AM) monomers and N,N-methylene-bis-(acrylamide)(MBA) as a crosslinker, Potassium peroxydisulfate (KPS) as initiator and N,N,N`,N`-tetramethylethylenediamine (TEMED) as an accelerator were purchased from Aldrich Chemical Company. MB was purchased from Sigma-Aldrich. Doubly Distilled Water (DDW) was used throughout the present work.

Preparations

Superparamagnetic Fe_3O_4 nanoparticles were prepared by chemical co-precipitation of iron (III) and iron (II) in an alkaline solution and then treating it under hydrothermal condition. In a typical experiment, 5.2 g of $FeCl_3.6H_2O$, 2 g of $FeCl_2.4H_2O$ and 0.85 ml HCl (12 mol/L) were dissolved in 25 ml of DDW (degassed with nitrogen gas before use) to prepare a stock solution. 250 ml of 1.5 mol/L NaOH solution was heated to 80°C in a beaker. The stock solution was added drop wise under nitrogen gas protection and vigorous stirring. After the reaction, the mixture was cooled to room temperature with stirring, and the resulting magnetic Fe_3O_4 nanoparticles were separated magnetically and washed with DDW four times to remove excess NaOH and finally dispersed in 100 ml DDW to be used for nanogel preparation.

Core shell poly(acrylamide-co-sodium acrylate) magnetic nanogel was prepared by solution polymerization. In a typical experiment, 1.52 g acrylamide, 1.54 g acrylic acid and 0.198 g MBA (3 mol% with respect to total monomer amount) were dissolved in 72 ml DDW in an ice cooled bath followed by addition of drops of 10 M NaOH till pH=9. The reaction system was bubbling nitrogen gas to exclude the air inside the flask for 20 minute, Then 75 ml of magnetite ferrofluid (10 mg/ml) was added under vigorous stirring. Afterwards, 3 ml aqueous

***Corresponding author:** Magda A Akl, Chemistry Department, Faculty of Science, Mansoura University, Mansoura, Egypt, E-mail: magdaakl@yahoo.com

Received April 28, 2013; **Accepted** May 27, 2013; **Published** June 01, 2013

Citation: Akl MA, Atta A, Youssef AEM, Ibraheim MA (2013) The Utility of Novel Superabsorbent Core Shell Magnetic Nanocomposites for Efficient Removal of Basic Dyes from Aqueous Solutions. J Chromat Separation Techniq 4: 185. doi:10.4172/2157-7064.1000185

solution of KPS (2 wt% with respect to total monomer amount) and 150 µl of TEMED were added to the solution to start polymerization. The reaction was carried out at room temperature under N_2 gas for 15 hour. After preparation of stable nanogel dispersion, the resultant polymer coated magnetic nanoparticles were collected with the aid of an external magnetic field, washed with DDW several times and finally dispersed in 45 ml DDW.

Sodium acrylate(Na-Ac) was prepared as following:12.01 g (0.3003 mol) NaOH and 10 ml water were added to a 50 ml Erlenmeyer flask equipped with a magnetic stirring bar, and the mixture was stirred to dissolution. The NaOH solution was carefully added to a 250 ml beaker containing 28.03 g (0.3893 mol) acrylic acid (exothermic reaction), with continuous stirring. The mixture was allowed to cool, 50 ml of acetone were added, and the precipitate vacuum filtered. The wet sodium acrylate was first air dried and subsequently dried in an oven at 55 C-60 C for 12-15 hours to obtain 27.31 g (96.8% yield) of sodium acrylate.

Superabsorbents nanocomposite hydrogels (Ac blank, Ac4% and Ac8%) containing 0, 4, 8 wt% of nanogel, respectively, were prepared by in situ free radical copolymerization of acrylamide and sodium acrylate in an aqueous dispersion of nanogel particles using MBA as crosslinker and KPS as the initiator. The total mass percentage of both monomers in the reaction mixture was 30%. In brief, to prepare a sample(S), 2.15 g of acrylamide, 2.84 g of sodium acrylate, 0.05 g of crosslinker MBA (1 wt % based on total monomer amount) were dissolved in water in an ice cooled bath under nitrogen atmosphere. Then, aqueous dispersion of magnetic nanogel particles was added to the mixture under vigorous stirring. Afterwards, 3 ml aqueous solution of initiator (0.05 g KPS, 1wt% with respect to total monomer amount) was added and the whole reaction mixture was transferred into a test tube (internal diameter 10 mm) and kept in an electric oven at 50°C for 10 hours. The hydrogel codes and complete compositions are listed in Table 1.

The formed nanocomposite hydrogels were recovered carefully by breaking the test tubes and cut into small disks of 3 mm thickness and 10 mm diameter. These hydrogel discs were safely transferred into DDW and allowed to equilibrate over a period of 5 days (water was repeatedly changed every 10 h) to remove unreacted monomers, crosslinker, initiator and soluble or un-crosslinked polymers, etc. Finally, the sample was dried in air followed by overnight drying in an electric oven to get completely dried gels and stored in airtight plastic bags.

Characterization

FTIR spectra were analyzed with a Nicolet FTIR spectrophotometer using KBr in a wavenumber range of 4000-5000 cm^{-1} with a resolution accuracy of 4 cm^{-1}. The images for magnetite and Fe_3O_4/p(Am-co-Na Ac) nanocomposites were recorded using High resolution transmission electron microscopy (HR-TEM) (JEM-2100F, JEOL, Japan) at an acceleration voltage of 120 kV. The surface morphologies of nanocomposite hydrogels were investigated using scanning electron microscopy (SEM, model JSM-T 220A, JEOL, Japan) equipped with an EDX detector. Zeta potential measurements of nanocomposite hydrogels were measured at different pH values using Laser Zeta meter Malvern Instruments Model Zetasizer 2000.

Sample code	Monomers feed molar ratio		MBA (g)	KPS (g)	Nanogel (wt %)
	Na-AC	Acm			
Ac blank	90	10	0.05	0.05	0
Ac 4%	90	10	0.05	0.05	4
Ac 8%	90	10	0.05	0.05	8

Table 1: Composition of nanocomposite hydrogels.

Adsorption studies

Batch sorption experiments were done by shaking 0.02 g of nanocomposite with 50 ml aqueous solution of MB in 250 ml-Erlenmeyer flasks placed in a temperature controlled shaking water bath at different concentrations (between 100 and 1600 mg/l), pHs (between 2 and 12), ionic strength (between 0.005 and 0.3 mole/l), temperatures (between 25°C and 45°C) and sorbent doses (between 0.01 and 0.05 g) at a constant shaking rate of 125 rpm. The concentration of MB in the residual solution was analyzed spectrophotometrically at 662 nm. The amounts of dye removed by superabsorbents (qe) and the percent of extraction (%E) are calculated using the following equations:

$$q_e = (C_o - C_e)/m \times 100 \quad (1)$$

$$\%E = (C_o - C_e)/C_o \times 100 \quad (2)$$

Where q_e is the amount of dye adsorbed (mg/g). C_o and C_e are the initial and equilibrium liquid-phase concentrations of dye (mg/g), respectively. V is the volume of the solution (l), and m is the weight of the sorbent used (g).

Results and Discussion

Characterization of adsorbents

The chemical structure of the prepared magnetite nanoparticles was confirmed by FT-IR analysis. The adsorption of AM, AA-Na and MBA as a ligand onto Fe_3O_4 colloidal nanoparticles clusters has been studied by means of FTIR. Figure 1 shows the FT-IR spectra of Fe_3O_4 nanoparticles, Ac blank, Ac 4% and Ac 8% nanocomposites. The FT-IR spectrum of Fe_3O_4 (Figure 1a) shows characteristic absorption band at 586 cm^{-1} corresponding to the Fe–O bond. Also, the presence of a band in the region of 3250-3600 Cm^{-1} indicates the presence of water of crystallization in the magnetite sample. The small peaks in the region 1500-1400 cm^{-1} can also be correlated to the different modes of bonded water molecules existing in the ferrofluid. In FT-IR spectrum of Ac 4% and Ac 8% nanocomposites (Figures 1b and 1c) there is shifting in ferrite peak by 15 Cm^{-1}. The shifting as well as broadening of the peaks

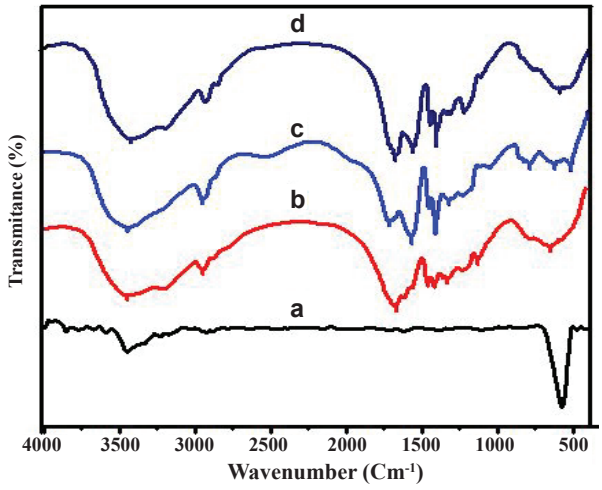

Figure 1: FTIR spectrum of (a) Fe_3O_4 nanoparticles, (b) Ac blank, (c) Ac 4%, and (d) Ac 8% superabsorbents.

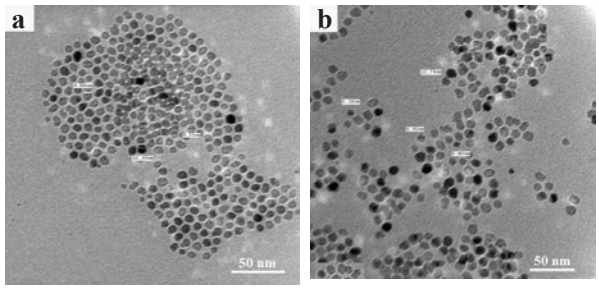

Figure 2: TEM of (a) Fe_2O_3 nanoparticles, and (b) core-shell magnetic nanogel.

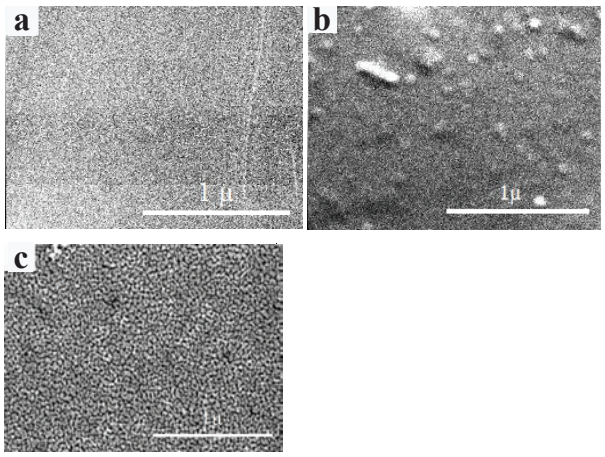

Figure 3: SEM images of (a) Ac blank, (b) Ac 4%, (c) Ac 8% nanocomposites, respectively.

can be attributed to interaction of 3d orbit of ferrite with N atom in AM to form coordinate bond [13]. In the FT-IR spectra of Ac blank, Ac 4% and Ac 8% (Figures 1b-d), the peaks found at 3400, 1650, and 1600 cm^{-1} indicate N–H stretching, C=O stretching and N–H bending of the amide bonds, respectively, which are characteristics of the–CONH group in the AM. In addition, the peak at 1411 cm^{-1} is due to the–C–N stretching, and the 765-710 cm^{-1} band represents the out of plane bending of the weak bond N–H. Based on the above observations, the Fe_3O_4 nanoparticles are located in the polymer shell.

The HR-TEM micrograph of the magnetite nanoparticles, Figure 2a, suggests that Fe_3O_4 nanoparticles are spherical in shape with mean diameter of 8 nm. Figure 2b confirms that the magnetic Fe_3O_4 nanoparticles coated with poly(Acrylamide-co-sodium acrylate) polymer are nanocapsules of spherical shape with an average diameter of 11 nm. On encapsulation with polymer, the size of the nanocapsules is increased from 8 to 11 nm. This is an indirect confirmation of the encapsulation of Fe_3O_4 magnetic core with a 3 nm thick polymer shell.

The morphologies of Ac blank, Ac 4%, Ac 8% nanocomposite, as observed by SEM, are shown in Figure 3. The pulverized Ac blank, obtained from the radical chain polymerization in aqueous solution, was essentially a smooth sheet free of any significant particulate nature (Figure 3a). The magnetic nanogel loadings at 4 and 8 %wt were immobilized in the Ac 4% and Ac 8% nanocomposite showed the nanogel particles to be well dispersed and so were found to reside on the surface and the inner depths (Figures 3b and 3c). The nanogel particle distribution increased with increasing nanogel content. The figures reveal that small spherical particles of 30 to 50 nm are imbedded within the polymer matrix with absence of phase separation or agglomerations of magnetic particles on the surface.

Zeta potential of Ac blank, Ac 4 % and Ac 8% has been investigated; the results are shown in Figure 4. It could be clearly seen that, with increasing the amount of nanogel on nanocomposite adsorbents the zeta potential shift to more negative values. So, Ac blank has less negative potential whereas Ac 8% has the highest negative potential. The presence of negatively charged carboxylate groups on the surface of nanogel is the main reason for shift in zeta potential to more negative values. This implies that the adsorption capacity of adsorbents toward positively charged MB will increase in the order Ac 8% Ac 4% Ac blank due to presence of more negatively charged active sites in that order. Also, the pH causes a dramatic change in zeta potential. As pH increase from pH 4 to pH 8, zeta potential increase from -20.7 to -29.7 mv, from -21.9 to -31.9 mv and from -22.8 to -36.1 mv for Ac blank, Ac 4% and Ac 8% respectively. With increasing the pH, zeta potential become more negative due to ionization of carboxylic group of acrylic acid. In contrast to that, as pH decrease, zeta potential decrease due to

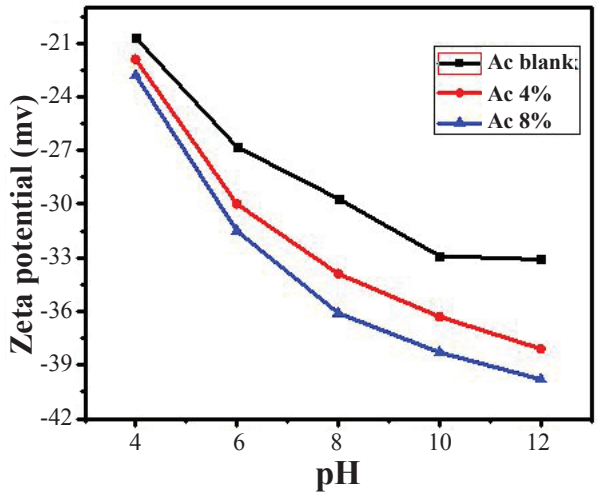

Figure 4: Zeta potential of Ac blank, Ac 4% and Ac 8% nanocomposites at different pH.

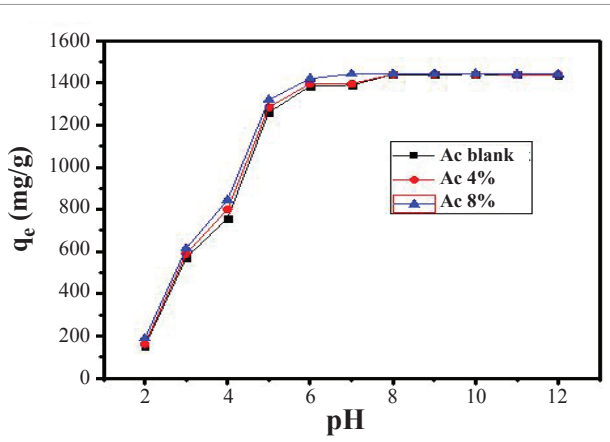

Figure 5: Effect of the pH values on adsorption capacity of MB by Ac blank, Ac 4% and Ac 8% nanocomposites. (Conditions: C_o=600 mg/l, T=25°C; adsorbent dose=0.02 g/50 ml).

conversion of —COO⁻ to —COOH and protonation of NH2 group of acrylamide.

Adsorption studies

Effect of pH: Figure 5 shows the effect of pH on the removal of MB onto Ac blank, Ac 4% and Ac 8% nanocomposites from aqueous solutions. The adsorption capacity of MB onto nanocomposite hydrogels increased significantly with increasing pH. The high adsorption capacity is due to the strong electrostatic interaction between the nanocomposite hydrogels and cationic dye molecules. Moreover, when pH value is increased, the carboxylic groups of the nanocomposites become ionized and the electrostatic repulsion between the molecular chains is predominated which leads to more expansion of the network and high adsorption of MB. When the pH increases from pH=3 to pH=4, The amount of MB adsorbed at equilibrium (q_e) increase from 570.38 to 1389.89 mg/g, from 590.64 to 1396.41 mg/g and from 614.68 to 1443.31 mg/g, for Ac blank, Ac 4% and Ac 8% nanocomposites, respectively. At acidic pH, the lower dye removal is probably due to the presence of excess H+ ions competing with positively charged MB molecules for the sorption sites of sorbents.

Effect of initial dye concentration: The effect of initial concentration on the removal of MB by Ac blank, Ac 4% and Ac 8% nanocomposites is shown in Figure 6. The adsorption capacities of the sorbents increase with an increase in initial dye concentration and the adsorption at different concentrations is rapid in the initial stages and gradually decreases with the progress of adsorption until the equilibrium is reached. This may be attributed to the fact that, the higher the initial MB concentration, the greater the driving force of the concentration gradient at solid-liquid interface which cause an increase of the amount of MB adsorbed on the adsorbent [16]. When the initial concentration of MB increases from 100 to 1000 mg/l at 25°C, the amount of MB adsorbed at equilibrium (q_e), increase from 244.54 to 2153.33 mg/g, from 244.87 to 2374.87 mg/g and from 248.23 to 2729.16 mg/g for Ac blank, Ac 4% and Ac 8%, nanocomposites, respectively. At higher MB concentrations adsorption capacity reached a plateau indicating saturation of the available binding sites on the adsorbent.

Effect of contact time: The adsorption capacity of Ac blank, Ac 4% and Ac 8% nanocomposites increased rapidly with the increase of contact time from 0 to 20 min (Figure 7) and more than 90% of the equilibrium adsorption capacity for MB occurred within 15 min. After 60 min, the adsorption capacity became constant and the adsorption reached equilibrium. Therefore, 60 min was selected as the contact time for the adsorption of MB onto the composites under our experimental conditions.

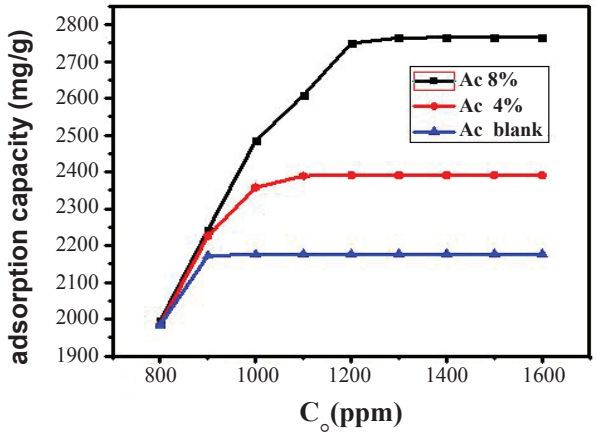

Figure 6: Effect of initial dye concentration on the removal of MB by Ac blank, Ac 4% and Ac 8% nanocomposites. (Conditions: T=25°C; adsorbent dose=0.02 g/50 ml; time=2 h).

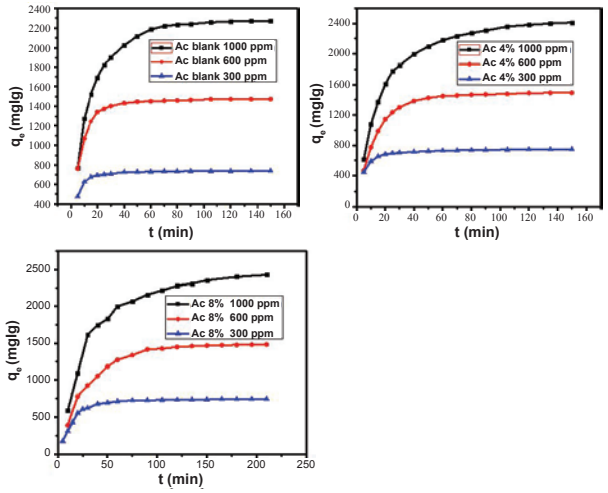

Figure 7: Effect of the contact time on adsorption capacity of Ac blank, Ac 4% and Ac 8% nanocomposites. (Conditions: T=25°C; adsorbent dose=0.02 g/50 ml; pH=7).

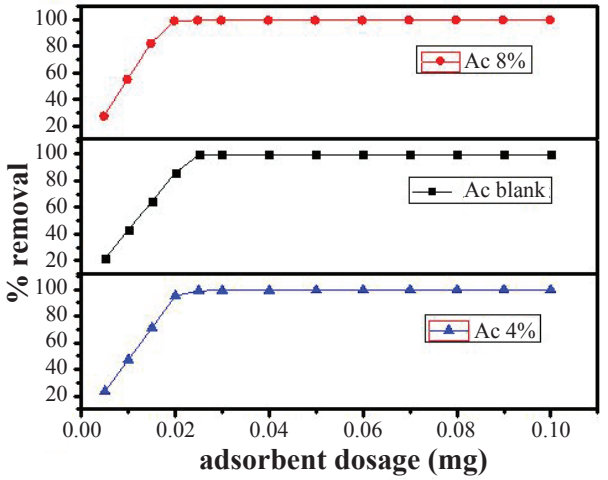

Figure 8: Effect of sorbent dosage on the removal of MB by Ac blank, Ac 4% and Ac 8% nanocomposites. (Conditions: T=25°C; C_o=1000 mg/l; time=2 h).

Effect of adsorbent dosage: When the sorbent dose increases from 0.01 to 0.02 g (Figure 8), the percent dye removals by Ac blank, Ac 4% and Ac 8% nanocomposites increase from 43.33% to 86.06%, from 47.30% to 95.21% and from 55.01% to 99.01%, respectively. This can be simply attributed to the increased sorbent surface area and availability of more sorption sites [17]. The decrease in adsorption capacity with increase in adsorbent dosage is due to the high number of unsaturated adsorption sites.

Effect of ionic strength: Figure 9 presents the effect of ionic strength on the uptake of MB. The adsorption capacity decreased with the increase in ionic strength. As the concentration of NaCl ions

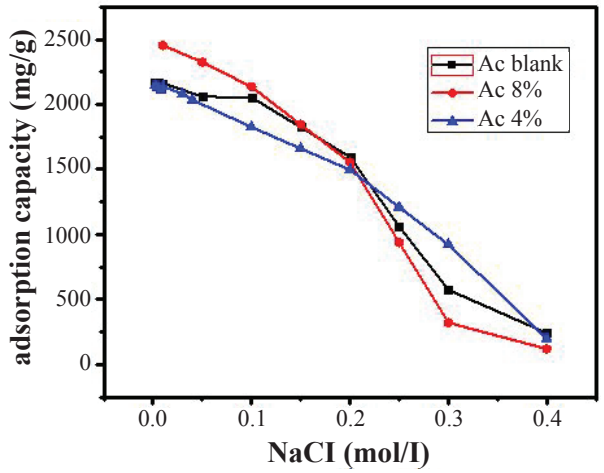

Figure 9: Effect of ionic strength on the removal of MB by Ac blank, Ac 4% and Ac 8% nanocomposites. (Conditions: T=25°C; adsorbent dose=0.02 g/50 ml; C_o=1000 mg/l; time=2 h).

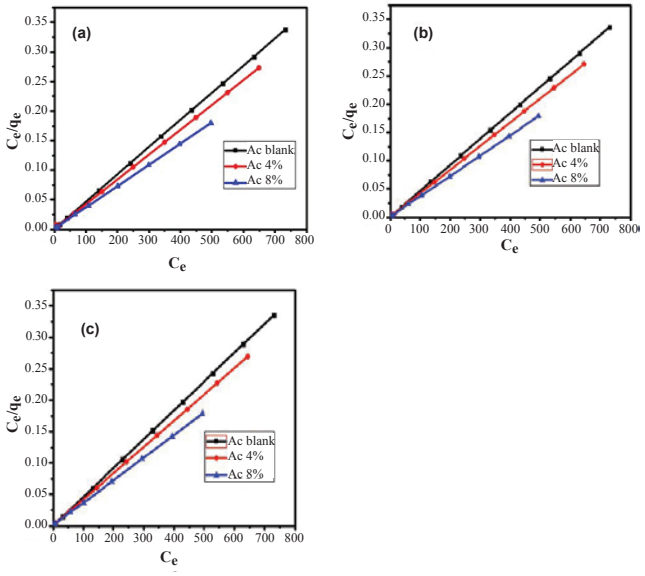

Figure 10: Langmuir plot for the adsorption of MB at (a) 25°C, (b) 35°C and (c) 45°C.

increased from 0.01 to 0.1 M, the adsorption capacities decreased from 2164.08 to 2053.215 mg/g, from 2137.772 to 1825.543 mg/g and from 2454.712 to 2136.364 mg/g for Ac blank, Ac 4% and Ac 8% nanocomposites, respectively. Further increase in ionic strength above 0.2 M lowers the adsorption capacities sharply until 0.4 M where any further increase cause steep decrease in adsorption capacities because of salting out of dye molecules from aqueous solution.

Effect of temperature: The adsorption capacity of the nanocomposites increased with increasing of the temperature from 25 to 45°C (Table 2). This is attributed to the increase in the kinetic energy of MB with increasing temperature and the flexibility of the hydrogel increases as well. Consequently, the rate of diffusion of MB molecules across the external boundary layer and in the internal pores in the nanocomposites increases with temperature [18], and the amount of MB uptake increases. When the temperature increased from 25°C to

Sample code	*Qe (mg g^{-1})*		
	25°C	**35°C**	**45°C**
Ac blank	2167.802	2171.987	2176.677
Ac 4%	2377.078	2384.123	2390.351
Ac 8%	2759.505	2763.716	2765.893

Table 2: Effect of temperature on maximum adsorption capacities of MB by Ac blank, Ac 4%, Ac 8%.

45°C, the maximum amounts of MB removed by Ac blank, Ac 4% and Ac 8% nanocomposites are found to be increased from 2167.802 to 2176.677 mg/g, from 2377.078 to 2390.351 mg/g and from 2759.505 to 2765.893 mg/g, respectively.

Adsorption isotherms

Adsorption is usually described through isotherms, that is, the amount of adsorbate on the adsorbent as a function of its pressure (if gas) or concentration (if liquid) at constant temperature. The two most common isotherm equations namely, Langmuir and Freundlich are tested here [19]. The Langmuir equation can be written as follows:

$$q_e = Q_0 K_l C_e / 1 + K_l C_e \quad (3)$$

Where qe is the amount of dye adsorbed on nanocomposites at equilibrium (mg/g), Q_0 is the maximum adsorption capacity (mg/g), K_l is the Langmuir constant, and C_e is the concentration of dye solution at equilibrium (mg/L). The linear form of Langmuir equation is:

$$C_e / q_e = 1 / Q_0 K_l + C_e / Q_0 \quad (4)$$

The monolayer adsorption capacity, Q and the Langmuir constant K_l can be obtained from the linear plot of C_e/q_e against C_e. An essential characteristic of Langmuir isotherm can be expressed by a dimensionless constant called equilibrium parameter, R_L [20], defined by:

$$R_l = 1 / 1 + K_l C_0 \quad (5)$$

Where C_0 is the highest initial dye concentration (mg/L), R_L values indicate the type of isotherm to be either unfavorable (R_L>1), linear (R_l=1), favorable (0<R_L<1) or irreversible (R_L=0) [21].

The Freundlich equation is given by [19]:

$$q_e = K_f C_e^{1/n} \quad (6)$$

Where K_F is the Freundlich constant which is a comparative measure of the adsorption capacity of the adsorbent, and n is an empirical constant which gives valuable information about the isotherm shape. 1/n values indicate the type of isotherm to be irreversible (1/n=0), favorable (0<1/n<1) and unfavorable (1/n>1).

The Freundlich parameters be obtained from the following linearized equation:

By linear plotting ln q_e as the function of ln C_e, the values of K_f and n can be obtained from the *slope* and the intercept of the plot.

$$\ln q_e = \ln K_f + 1 / n \ln C_e \quad (7)$$

Figures 10 and 11 show the linear plot of Langmuir and Freundlich isotherms for adsorption of MB on nanocomposites. The model parameters obtained by applying Langmuir and Freundlich models to the experimental data are given in Tables 3 and 4. The regression coefficients R^2 obtained from Langmuir model are closer to 1 suggesting that the Langmuir isotherm fits better with the adsorption of MB on Ac blank, Ac 4% and Ac 8% nanocomposites. In addition, the q_{max} values for the adsorption of MB onto the nanocomposites calculated from the

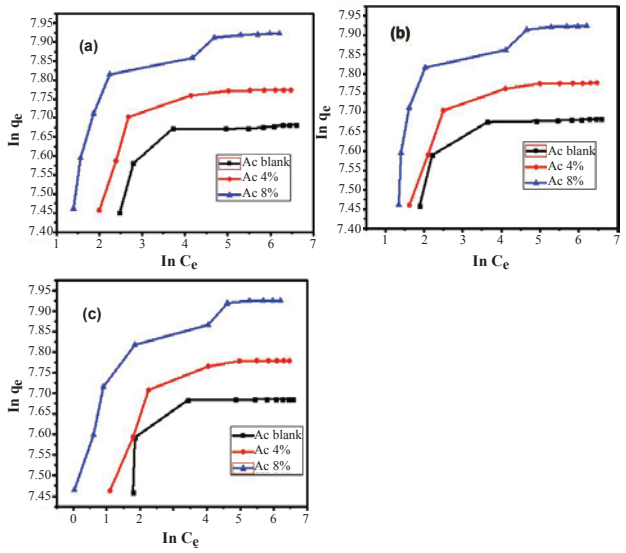

Figure 11: Freundlich plot for the adsorption of MB at (a) 25°C, (b) 35°C and (c) 45°C.

Sample Code	T (°C)	$Q_{e,exp}$ (mg g^{-1})	$Q_{max, Fitted}$ (mg g^{-1})	K_L (L mg^{-1})	Ln K_L (L mol-1)	R^2
Ac blank	25	2167.802	2173.435	0.4745	11.9301	0.9999
	35	2171.987	2174.811	0.9123	12.5838	1
	45	2176.677	2178.910	1.7867	13.2559	1
Ac 4%	25	2377.078	2403.5053	0.191732	11.02395	0.9996
	35	2384.123	2401.1795	0.28921	11.435	0.9998
	45	2390.351	2399.2322	0.610744	12.18253	0.9999
Ac 8%	25	2759.505	2771.7953	0.4673	11.91473	0.9999
	35	2763.716	2774.9720	0.5404	12.06022	0.9999
	45	2765.893	2772.8021	0.9319	12.60508	0.9999

Table 3: Langmuir isotherm parameters and correlation coefficient for adsorption of MB by Ac blank, Ac 4%, Ac 8% at different temperatures.

Sample Code	T (°C)	1/n	Ln K_f	R^2
Ac blank	25	0.03912	7.44614	0.6006
	35	0.03425	7.48023	0.63252
	45	0.03177	7.49916	0.5780
Ac 4%	25	0.23825	6.49468	0.55408
	35	0.21875	6.61173	0.55314
	45	0.1957	6.75972	0.58564
Ac 8%	25	0.02935	7.75168	0.88331
	35	0.02785	7.76279	0.88524
	45	0.02652	7.773	0.87547

Table 4: Freundlich isotherm parameters and correlation coefficient for adsorption of MB by Ac blank, Ac 4%, Ac 8% at different temperatures.

Langmuir model are all the same as the experimental data. Also, R_L values obtained are in the range of 0.1195-0.2534, thereby confirming that the adsorption is a favorable process. It can be concluded that the monolayer Langmuir adsorption isotherm is more suitable to explain the adsorption of MB onto the proposed nanocomposites.

Adsorption kinetics

The pseudo-first order kinetic model was suggested by Lagergren its linear form can be formulated as

$$\log[(q_e - q_t)] = \log q_e - K_1 t / 2.303 \quad (8)$$

Where q_e is the adsorption uptake of MB at time t (mol g^{-1}) and

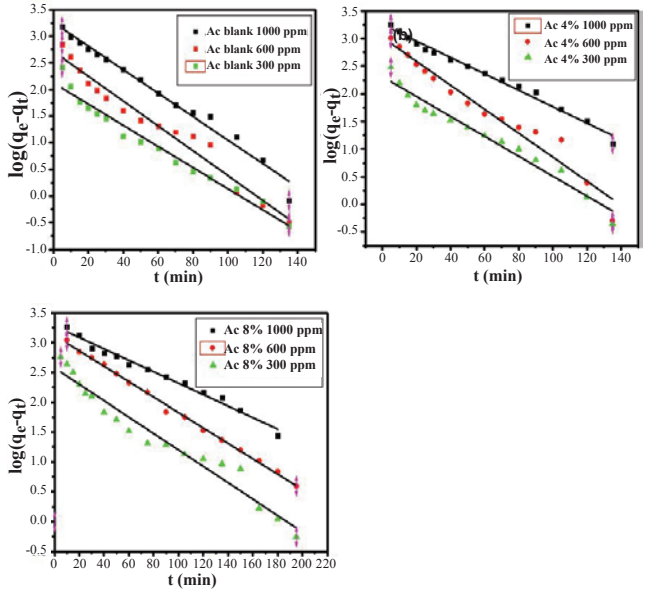

Figure 12: Pseudo-first-order kinetic model.

Sample code	C_o	$q_{e,cal}$	K	R^2
Ac blank	1000	1816.519	0.05087	0.98013
	600	524.3484	0.05382	0.96391
	300	133.3828	0.04581	0.96653
Ac 4%	1000	1791.637	0.03422	0.98686
	600	1053.416	0.04998	0.95768
	300	205.0548	0.0415	0.96405
Ac 8%	1000	1907.129	0.02211	0.9828
	600	1323.64	0.02978	0.99697
	300	377.3896	0.03167	0.95513

Table 5: First order kinetic parameters for adsorption of MB by Ac blank, Ac 4%, Ac 8% at different concentrations.

k1 (min^{-1}) is the rate constant of the pseudo-first-order adsorption. A plot of log (q_e-q_t) versus t should be linear; the parameters k_1 and R^2 (correlation coefficient) calculated from the data (Figure 12) are listed in Table 5. The large differences between the experimental q_e values ($q_{e,exp}$) and the calculated q_e values ($q_{e,ca}$l) indicate that the pseudo-first order kinetic model was poor fit for the adsorption processes of Ac blank, Ac 4% and Ac 8% nanocomposites for MB.

The Ho's pseudo-second-order kinetic model [22] can be expressed as:

$$t / q_t = 1 / K_2 q_e^2 + t / q_e \quad (9)$$

Where k_2 (g $mol^{-1}min^{-1}$) is the rate constant of pseudo-second-order adsorption. Figure 13 shows the plot of *t/q* versus *t* for MB onto Ac blank, Ac 4% and Ac 8% nanocomposites. The correlation coefficients(R^2), Table 6, for the pseudo-second order kinetic model are all over 0.9999, moreover, the qe,cal values for the pseudo-second order kinetic model are all consistent with the $q_{e,exp}$ values. These findings suggest that the adsorption processes of Ac blank, Ac 4% and Ac 8% nanocomposites for MB can be well described by the pseudo-second order kinetic model.

The intra-particle diffusion parameter, K_p (mmol.g^{-1} $h^{-0.5}$) is defined by equation:

$$q_t = K_p t^{0.5} + C \quad (10)$$

Where k_p is the intra-particle diffusion rate constant (mmol.g^{-1} $h^{-0.5}$)

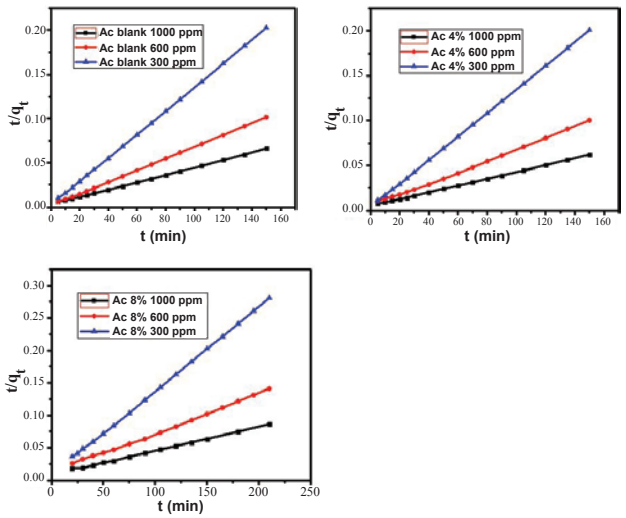

Figure 13: Pseudo-second-order kinetic model.

Sample code	*C₀*	k_2 (g mg^{-1} min^{-1})	$q_{e,cal}$ (mg g^{-1})	*R²*
Ac blank	1000	0.4943	2428.5638	0.99926
	600	2.2354	1510.7657	0.99971
	300	7.6909	751.8797	0.99992
Ac 4%	1000	0.2753	2653.0055	0.99948
	600	0.7798	1595.0693	0.99836
	300	4.8753	763.3588	0.99996
Ac 8%	1000	0.1334	2775.8039	0.99585
	600	0.2634	1682.6802	0.99577
	300	1.2721	793.6508	0.9978

Table 6: Second order kinetic parameters for adsorption of MB by Ac blank, Ac 4%, Ac 8% at different concentrations.

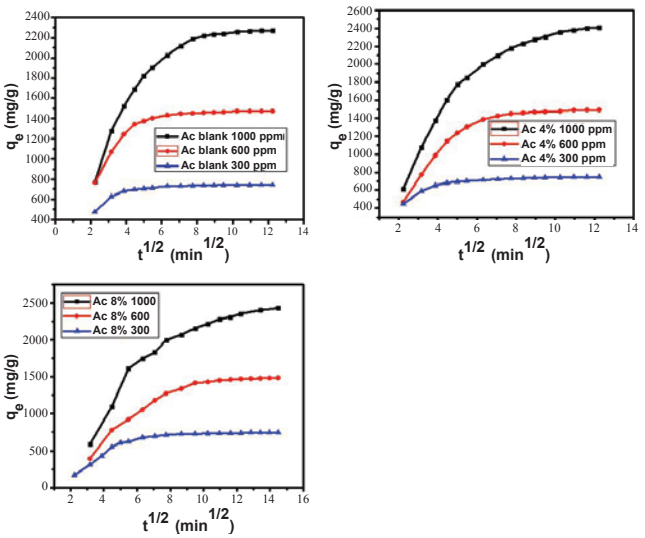

Figure 14: Intra-particle diffusion plots.

and *C* is a constant. According to this model q_t versus $t^{0.5}$ should be linear if intra-particle diffusion is involved in the adsorption process [23]. From Eq. (5), if pore diffusion is the rate limiting step, then a plot of q_t against $t^{0.5}$ must give a straight line with a slope that equals k_p and the intercept value c represents the resistance to mass transfer in the external liquid film.

Figure 14 shows the plot of q_t against $t^{0.5}$ of Ac blank, Ac 4% and Ac 8% nanocomposites for MB at three different initial concentrations; the plots are multi-linear, containing at least three linear segments which indicate that three steps occur during adsorption process. The first sharper portion is the transport of dye molecules from the bulk solution to the adsorbent external surface by diffusion through the boundary layer (film diffusion). The second portion is the diffusion of the dye molecules from the external surface into the pores of the adsorbent. The third portion is the final equilibrium stage, where the dye molecules were adsorbed on the active sites on the internal surface of the pores and the intra-particle diffusion starts to slow down due to the solute concentration getting lower and lower in solution [24]. The linear portions of curves did not pass through the origin, suggesting that pore diffusion is not the step controlling the overall rate of mass transfer at beginning of adsorption.

Thermodynamic studies

The data obtained from the temperature studies were used for thermodynamic analysis. The Gibbs free energy is presented in Eq. (12). The Gibbs free energy can also be expressed using enthalpy and entropy at a constant temperature. The linearized form of Eqs. (11) and (12) results in Eq. (13), which is the Van't Hoff equation [25]:

$$\Delta G^{o} = RT \ln K_c \quad (11)$$

$$\Delta G^{o} = \Delta H^{o} - T\Delta S^{o} \quad (12)$$

$$\ln K_c = \Delta S / R - \Delta R K_l / RT \quad (13)$$

where ΔG° (kJ/mol) is the change in Gibbs Free Energy, ΔH° (kJ/mol) is the enthalpy change of MB adsorption, ΔS° (J/mol K) is the entropy change of MB adsorption, R is the universal gas constant (8.314J/mol K), T is the absolute temperature (K), and K_l is the Langmuir constant.

By plotting a graph of ln K_c versus 1/T (Figure 15), the values of ΔH° and ΔS° can be estimated from the slope and intercept of Van't Hoff plots, respectively. The thermodynamic parameters are given in Table 7 and 8. The negative values of ΔG° for Ac blank, Ac 4% and Ac 8% nanocomposites at various temperatures indicate the spontaneous nature of the sorption process. The fact that the values of the ΔG° decrease with increasing temperature indicates the increase of spontaneous effect. For all sorbents, the positive value of ΔH° suggested the endothermic nature of the adsorption process (Tables 9

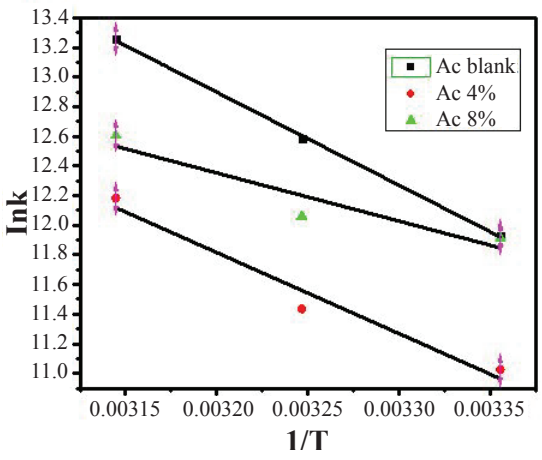

Figure 15: The plots of lnKa versus T^{-1} for estimations of thermodynamic parameters.

Sample code	C_o	K(mg g-1 min-0.5)	R^2
Ac blank	1000	375.68769	0.96163
	600	261.21426	0.97107
	300	127.78369	0.92865
Ac 4%	1000	421.3177	0.99132
	600	303.93001	0.99621
	300	106.87931	0.92895
Ac 8%	1000	384.32703	0.96557
	600	185.944	0.9686
	300	162.28759	0.99397

Table 7: Intraparticle diffusion parameters for adsorption of MB by Ac blank, Ac 4%, Ac 8% at different concentrations.

Sample Code	ΔH° (KJ/mol)	ΔS° (KJ/mol K)	ΔG° (KJ/mol)		
			298 K	308 K	318 K
Ac blank	52.2015	0.2742	- 29.5576	-32.2234	- 35.0466
Ac 4%	45.4809	0.243	-27.3126	-29.2817	-30.1830
Ac 8%	27.0154	0.1891	-29.5196	-30.8827	-33.3259

Table 8: Thermodynamic parameters for adsorption of MB by Ac blank, Ac 4%, Ac 8% at different temperatures.

C_o	q_e for first cycle (mg/g)	q_e for second cycle (mg/g)	
		Treatment with HNO_3	Treatment with NaOH
300	748.20	481.23	748.15
400	997.43	486.95	994.43
500	1246.81	495.61	1234.34

Table 9: The adsorption capacity of MB using Ac 8% nanocomposite before and after treatment with NaOH at three different concentrations.

C_o	Regeneration efficiencies in each cycle (%)		
	2nd	3rd	4th
300	100	99.9	99.9
400	99.7	99.3	98.1
500	99	98.4	97.1

Table 10: Regeneration efficiencies of Ac 8% nanocomposite after repeated adsorption desorption cycles.

and 10). Moreover, the positive values of ΔS° point out the increased randomness at the solid/liquid interface during the sorption of MB on Ac blank, Ac 4% and Ac 8% nanocomposites.

Conclusion

The results of the present study reveals that Fe_3O_4/poly (Acrylamide-co-sodium acrylate) core shell magnetic nanogel (Fe_3O_4/p(Am-co-Na Ac)) based on crosslinked poly (sodium acrylate-co-acrylamide) may be an extremely viable adsorbent for application in the treatment of water and industrial wastewater contaminated with dyes. The amount of MB adsorbed was found to increase with increasing the wt% of nanogel from 4% to 8%. Moreover, the adsorption of MB was dependent on initial concentration, reaction temperature and pH. The MB adsorption capacity increased with the increase of pH in the range of 3–8, where ionization of carboxylic group occurs. The adsorption of MB onto the nanocomposites reached equilibrium within about 60 min. The adsorbents exhibited high sorption capacities toward basic dyes, viz.: 2167.802-2765.893 mg g^{-1}. The adsorption equilibrium could be well described by Langmuir adsorption isotherms, namely monolayer adsorption on a homogenous surface. The adsorption kinetics followed a pseudo-second order kinetic model and intra-particle diffusion was involved in the adsorption process. Thermodynamic results indicated that the adsorption process was spontaneous and endothermic in nature.

Acknowledgement

The author would like to thank Dr MAGabr providing drug samples.

References

1. Sanghi R, Bhatttacharya B, Singh V (2002) Cassia angustifoliaseed gum as an effective natural coagulant for decolourisation of dye solutions Green Chem 4: 252-254.
2. Ghosh D, Bhattacharyya KG (2002) Adsorption of methylene blue on kaolinite. App Clay Sci 20: 295-300.
3. Kornaros M, Lyberatos G (2006) Biological treatment of wastewaters from a dye manufacturing company using a trickling filter. J Hazar Mater 136: 95-102.
4. Guibal E, Roussy J (2007) Coagulation and flocculation of dye-containing solutions using a biopolymer (Chitosan). React and Func Pol 67: 33-42.
5. Zhao W, Wu Z,Wang D (2006) Ozone direct oxidation kinetics of Cationic Red X-GRL in aqueous solution. J Hazar Mater 137: 1859-1865.
6. Dutta K, Mukhopadhyay S, Bhattacharjee S, Chaudhuri B (2001) Chemical oxidation of methylene blue using a Fenton-like reaction J Hazar Mater 84: 57-71.
7. Capar G, Yetis U, Yilmaz L (2006) Membrane based strategies for the pre-treatment of acid dye bath wastewaters, J Hazar Mater135: 423-430.
8. Liu CH, Wu JS, Chiu HC, Suen SY, Chu KH (2007) Removal of anionic reactive dyes from water using anion exchange membranes as adsorbers. Water res 41: 1491-1500.
9. Muruganandham M, Swaminathan M (2006) TiO2-UV photocatalytic oxidation of Reactive Yellow 14: Effect of operational parameters. J Hazard Mater 135: 78-86.
10. De Lisi R, Lazzara G, Milioto S, Muratore N (2007) Adsorption of a dye on clay and sand. Use of cyclodextrins as solubility-enhancement agents. Chemosphere 69: 1703-1712.
11. Dabrowski A (2001) Adsorption--from theory to practice. AdvColl Inter Sci 93: 135-224.
12. Ahmad A, Rafatullah M, Danish M (2007) Sorption studies of Zn (II)-and Cd (II) ions from aqueous solution on treated sawdust of wood. Eur J Wood and Wood Prod 65: 429-436.
13. Xie G, Zhang Q, Luo Z, Wu M, Li T (2003) Preparation and characterization of monodisperse magnetic poly (styrene butyl acrylate methacrylic acid) microspheres in the presence of a polar solvent, J appl pol sci 87: 1733-1738.
14. Lee Y, Rho J, Jung B (2003) Preparation of magnetic ion-exchange resins by the suspention polymerization of styrenewith magnetite. J appl pol sci89: 2058-2067.
15. Hameed B (2009) Removal of cationic dye from aqueous solution using jackfruit peel as non-conventional low-cost adsorbent. J Hazar Mater 162: 344-350.
16. Ho YS, Chiang TH, Hsueh YM (2005) Removal of basic dye from aqueous solution using tree fern as a biosorbent. Prod Biochem 40: 119-124.
17. Garg V, Amita M, Kumar R, Gupta R (2004) Basic dye (methylene blue) removal from simulated wastewater by adsorption using Indian Rosewood sawdust: a timber industry waste. Dyes and pig 63: 243-250.
18. Özer A, Akkaya G, Turabik M (2006) Biosorption of Acid Blue 290 (AB 290) and Acid Blue 324 (AB 324) dyes on Spirogyra rhizopus. J Hazard Mater 135: 355-364.
19. Arami M, Limaee NY, Mahmoodi NM, Tabrizi NS (2006) Equilibrium and kinetics studies for the adsorption of direct and acid dyes from aqueous solution by soy meal hull. J Hazard Mater 135: 171-179.
20. Webi TW, Chakravort RK (1974) Pore and solid modes for fixed adsorbers. AIChEJ 20: 228-238.
21. Mckay G (1982) Adsorption of dyestuffs from aqueous solutions with activated carbon I: Equilibrium and batch contact-time studies. J Chem Techn and Biotechn 32: 759-772.

22. Ho Y, McKay G (1998) A Comparison of Chemisorption Kinetic Models Applied to Pollutant Removal on Various Sorbents. Process Safety and Environmental Protection 76: 332-340.

23. Kiran I, Akar T, Ozcan A, Tunali S (2006) Biosorption kinetics and isotherm studies of Acid Red 57 by dried Cephalosporiumaphidicola cells from aqueous solutions. Biochem Engin J 31:197-203.

24. Sun Q, Yang L (2003) The adsorption of basic dyes from aqueous solution on modified peat-resin particle. Water res 37: 1535-1544.

25. Hameed B, El-Khaiary M (2008) Kinetics and equilibrium studies of malachite green adsorption on rice straw-derived. Char J Hazar Mater 153: 701-708.